Chapter 3
Lead-Free Dielectrics: A State-Of-The-Art for Green Energy Storage

Swetapadma Praharaj and Dibyaranjan Rout

1 Introduction

With greater advancements in science and technology, the lifestyle and lifespan of the human race are improving which has lead to problems like overpopulation and excessive use of energy. A survey speaks that the global energy consumption has increased from 54,207 TWh in 1973 to 111,125 TWh in 2016 [1] and is expected to increase much more in the future. The present demands for energy probably arise from higher living standards, reduction in poverty, and decreasing mortality rates. As per a review published by Robert Rapier in Forbes magazine in June 2020, fossil fuels including coal, natural gas, and petroleum cater to at least 84% of world energy needs [2]. Not only it is creating global warming and air pollution but also leading to the fast depletion of fossil fuels. Hence there is an urgent surge to shift our energy dependence from fossil fuels to cleaner and greener renewable sources such as solar, wind, tidal, geothermal, etc. However, most of the renewable sources are intermittent which poses challenges in harnessing them as and when needed. Conversion of renewable energy into other reliable forms (usually electricity) might be one of the feasible solutions to overcome the above-mentioned insecurities by implementing efficient and reliable electrical energy storage systems. Several energy storage technologies such as batteries, solid oxide fuel cells (SOFC), electrochemical capacitors (ECs), flywheels, superconducting magnetic energy storage (SMES), and electrostatic/dielectric capacitors have brought a path-breaking revolution in this area of interest. Though all of these systems are quite efficient, none of them fulfill the conditions of both high energy density and power density simultaneously. Ragone

S. Praharaj · D. Rout (✉)
Department of Physics, School of Applied Sciences, KIIT Deemed to be University, Bhubaneswar 751024, Odisha, India
e-mail: droutfpy@kiit.ac.in

S. Praharaj
e-mail: spraharajfpy@kiit.ac.in

B. P. Swain (ed.), *Advances in Nanostructured Materials*, Materials Horizons: From Nature to Nanomaterials, https://doi.org/10.1007/978-981-16-8391-6_3

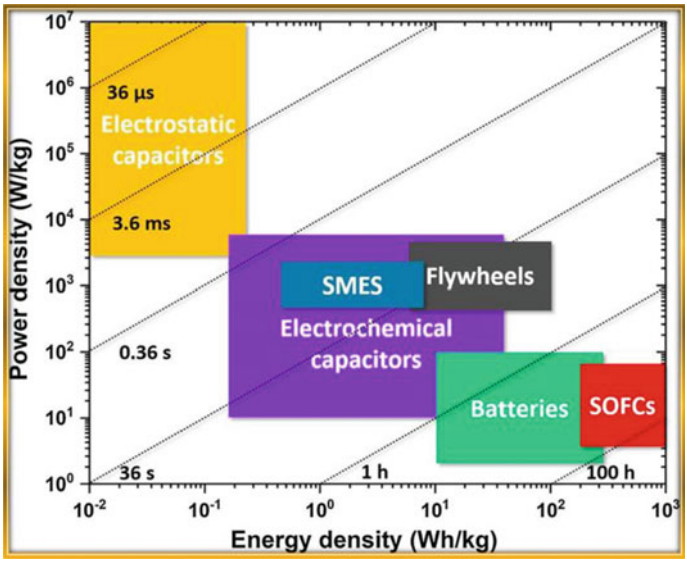

Fig. 1 Ragone plot comparing different energy storage devices: electrostatic capacitors, superconducting magnetic energy storage systems (SMES), electrochemical capacitors, flywheels, batteries, and solid oxide fuel cells (SOFCs) [3]

plot (Fig. 1) seems to be useful and is widely used in benchmarking the performance of the presently known energy storage devices based on a relative graph between energy density and power density.

While batteries and fuel cells demonstrate high energy density and low power density, dielectric capacitors exhibit contrasting features. Meanwhile, ECs possess medium energy and power density but suffer from large leakage current (~mA), low operating voltage (<3 V) and involves a high cost (9500 USD/kWh) [4, 5]. Dielectric capacitors are found to be most suitable for cost-effective, high voltage, and large-scale applications with their unique properties of faster charge–discharge rates (~ns) and fairly good power density (up to 10^8 W/kg). Such unique properties make them appropriate for super high power electronic systems such as medical defibrillators, electrical weapons, spacecraft, satellites, hybrid electric vehicles as shown in Fig. 2. They occupy almost 25% of the volume and weight of portable and power electronics as well as pulsed power systems.

One of the disadvantages of the dielectric capacitors is relatively low energy density as shown in Fig. 1. Thus it is very important to elevate the energy density of the dielectric materials used in capacitors as it will enhance the volumetric efficiency of the devices benefitting the miniaturization and easy integration of consumer electronics. For most of these applications, we rely on lead-based materials due to their unsurpassed performances which have inevitably invited environmental concerns. Blindly addressing the energy issues by neglecting lead emission would be accompanied by secondary damage to the mother earth. To plausibly elevate the energy

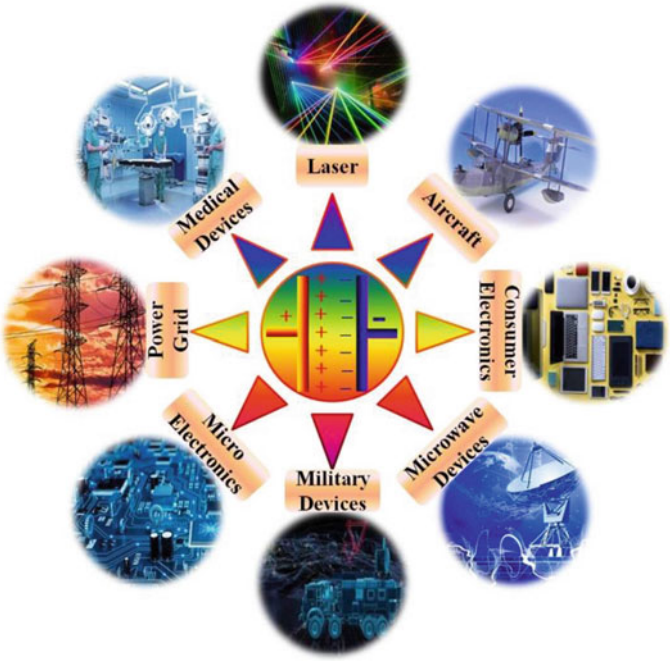

Fig. 2 Various applications of dielectric capacitors as energy storage devices

crisis without secondary Pb pollution, lead-free dielectric could be possibly the best solution for energy storage capacitors. In this chapter, we would draw the attention of the readers to the importance of lead-free dielectric materials from a capacitor point of view and record the probable measures of enhancing their storage performance.

2 Fundamentals of Dielectric Energy Storage in Capacitors

A typical dielectric capacitor is designed by sandwiching a dielectric layer between two conductive metal plates (e.g., Ag, Au, or Pt) as electrodes. The energy storage capability of the dielectric layer is determined in terms of capacitance given by the basic equation:

$$C = \frac{\varepsilon_0 \varepsilon_r A}{d}, \tag{1}$$

where ε_0 is the dielectric permittivity of free space (8.85 X 10^{-12} F/m); ε_r is the relative permittivity (or dielectric constant) of the dielectric material; A denotes the overlapping area of both the electrodes, and d is the thickness of the layer. The

capacitance is independent of the potential difference between the plates and charges stored on it but depends only on the geometry of the capacitor and the permittivity of the dielectric layer.

On applying an external voltage V, positive and negative charges start accumulating on the plates which are conventionally known as the charging process. Charging creates an internal electric field that is opposite in direction to the externally applied field. Piling up of the charges on the capacitor plates leads to an increase in the internal field and finally this process ends up when the internal electric field comes at par with the applied field. Supposing that charges $+Q$ reside on the capacitor plate, then the capacitance is given by Q/V. Many a time it is found that the relative permittivity of the dielectrics is affected by the external bais which in turn alters the capacitance. In such cases, capacitance may be expressed in terms of incremental variation:

$$C = \frac{dq}{dv} \tag{2}$$

During the charging process, work is done by the applied field in moving the charges and hence electrostatic energy is stored is dielectric and can be calculated as

$$W = \int_0^{Q_{\max}} V dq, \tag{3}$$

where Q_{max} is the maximum stored charge and dq is the incremental change in charge stored.

One of the salient figures of merit for energy storage dielectric capacitors is the total energy density (J) defined as energy stored per unit volume and is expressed as

$$J = \frac{W}{Ad} = \frac{\int_0^{Q_{\max}} V dq}{Ad} = \int_0^{D_{\max}} E dD, \tag{4}$$

where D refers to the electric displacement in the dielectric layer under the corresponding electric field E. In the case of dielectrics with high relative permittivity, the electric displacement $D(= \varepsilon_0 \varepsilon_r E)$ is very close to the polarization P. Hence Eq. (4) may be rewritten as

$$J = \int_0^{P_{\max}} E dP = \int_0^{E_{\max}} \varepsilon_0 \varepsilon_r E dE \tag{5}$$

Here E_{max} is the maximum electric field induced by the charges accumulated during the charging process.

The actual charge stored is usually determined by J_{res} (recoverable energy density) rather than J and is illustrated as

$$J_{rec} = \int_{P_r}^{P_{\max}} E\,dP \tag{6}$$

The energy storage efficiency for the dielectric material can be calculated as

$$\eta = \frac{J_{rec}}{J} \tag{7}$$

The above equations signify that both J and J_{rec} can be derived from polarization versus electric field ($P - E$) loops [6] as shown in Fig. 3a-f.

In the figure, we highlight four types of dielectric materials. The first category is linear dielectric in which the permittivity is independent of electricity due to the absence of domain structure. Hence Eq. (5) reduces to

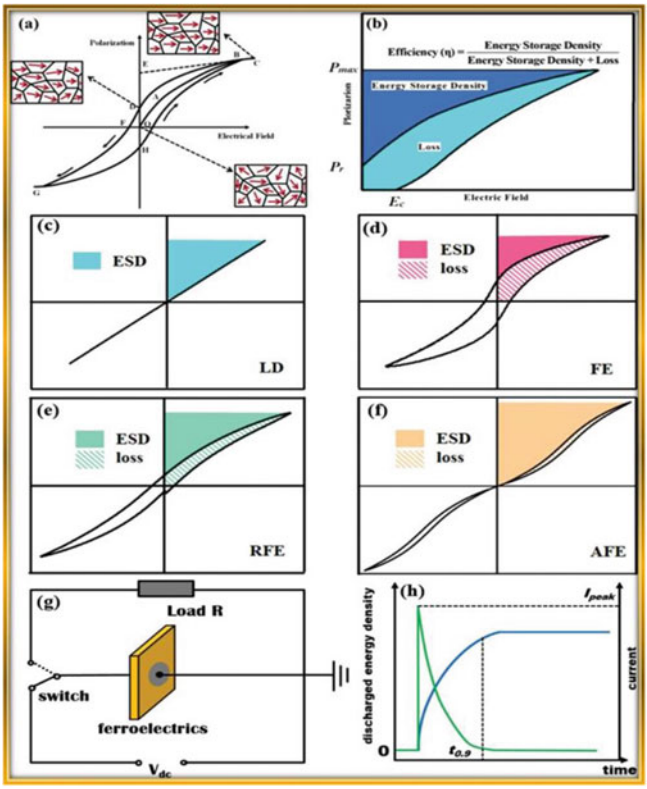

Fig. 3 **a** Switching of ferroelectric domains during the charge–discharge cycle; **b** Schematic of energy storage density (ESD) and efficiency (η) shown in P–E loop; **c-f** Schematic of ESD and loss in linear dielectric (LD), ferroelectrics (FE), relaxor ferroelectrics (RFE) and antiferroelectrics (AFE) respectively; **g** Basic circuit for measuring discharge energy density; **h** Discharge energy density and current as a function of time [7]

$$J = \frac{1}{2}\varepsilon_0 \varepsilon_r E^2 \tag{8}$$

The second group refers to the ferroelectric materials (FE) which have a well-defined domain structure. The most typical feature of this group of materials is the existence of a non-linear relationship between polarization and electric field giving rise to a square hysteresis loop. This is caused by the switching of the domain polarization direction with the direction and magnitude of the applied field. As such growth, disappearance, and domain wall displacements greatly influence the structure and electrical properties of ferroelectric materials, the third and fourth categories consisting of relaxor ferroelectrics (RFE) and antiferroelectrics (AFE) are both subgroups of FEs. Relaxor ferroelectrics containing polar nano regions (PNRs) show the ease of domain/domain wall motion leading to slimmer *P–E* loops and enhanced energy storage density. RFEs exhibit a unique feature of diffuse phase transition which ensures better thermal stability [8]. On the contrary, in the case of AFEs polarization and electric field follow a linear relationship below a certain critical electric field Ec. However, the loop becomes non-linear above Ec. The existence of two sets of lattice structures with opposite polarization directions in antiferroelectric leads to double *P–E* loops. Such a peculiarity is responsible for high energy storage density for AFEs.

The above-discussed methodology of ascertaining the energy storage density is often referred to the as quasistatic method. There is yet another approach to measuring the storage density called the dynamic method. In this procedure, the discharged energy density is derived from charge–discharge measurements. At first, a capacitor with the sample dielectric is charged by the applied external bias, and charges are stored on the capacitor plates. Then the same capacitor is allowed to discharge through an appropriate load resistor R_L. All this is carried out in a simple switching circuit (MOSFET is used as the electronic switch) as shown in Fig. 3g. If $I(t)$ and $V(t)$ are the voltage and currently recorded in R_L at any instant of time t during the discharging process, then the discharged energy density is (J_{dis}) is given by

$$J_{dis} = \frac{\int R_L I^2(t)dt}{V_{vol}} = \frac{\int V^2(t)dt}{R_L V_{vol}}, \tag{9}$$

where V_{vol} refers to capacitor volume. It is important to note that $R_L >>$ equivalent series resistor of the capacitor so that maximum stored energy can be delivered to the load resistor and the estimated discharge energy density is almost equal to the stored energy density [9]. Nevertheless, the energy density (in the dynamic method) is determined by calculating the integrated area in the *P–E* loop and is often more than that obtained by the charge–discharge method [10, 11]. Such kind of inconsistency may be ascribed to diverse mechanisms of *P–E* loops and dynamic discharge current at different frequencies [11, 12]. It is a usual practice to measure the *P–E* loops under low frequencies, i.e., on a scale of milliseconds. On the other hand, charge–discharge measurements are carried out on a microsecond scale. At higher frequencies of an electric field, domains/domain walls are clamped due to which their switching is

hindered leading to more energy loss. This phenomenon is more pronounced in the case of materials with macro-sized domain structure, i.e., FE and AFE. However curbing the domain size to nano-level (as in the case of RFE) facilitates faster and easier domain wall motion reducing the energy loss to a greater degree [13]. Hence the charge–discharge method is more suitable for assessing the performance of capacitors used in pulse power applications where they need to release the stored energy in the shortest possible time. Maximum current I_{peak} during the discharging process and $t_{0.9}$ (Fig. 3h) representing the 90% of discharge time are generally employed to characterize the energy storage capabilities of capacitors for high power and pulse power applications under a given load resistor [13–15]. Besides, *P–E* loop method is appropriate for estimating the performance of the material itself since the domains can switch their polarization direction fairly well under low-frequency measurements.

Apart from energy density, there are few other application-oriented figures of merit for capacitor materials include power density and dielectric breakdown strength (for high pulse power capacitors); ripple current capability, equivalent series resistance, and RC constant (for coupling capacitors).

3 Energy Storage in Lead-Free Materials: Bulk to Nano

3.1 Ferroelectrics

Ferroelectrics are materials featured by a finite polarization even in the absence of an external electric field. This polarization switches reversibly between two stable states depending on the direction of an applied field. These localizations of different polarization co-exist inside the FE materials are conventionally known as FE domains [16]. The switching behavior of the ferroelectric domains is studied experimentally with the help of *P–E* loops giving rise to the fingerprint square hysteresis loop. FEs with high dielectric permittivity are often associated with high dielectric loss and large remnant polarization yielding low values of recoverable energy density and dielectric breakdown strength. Thus it can be said that conventional ferroelectrics are not quite appropriate for energy storage. However, in recent times, many modifications have been proposed by different researchers to improve the energy storage capability of classical ferroelectrics. Some of the potential lead-free candidates identified in this regard include $BaTiO_3$ (BT), $SrTiO_3$ (ST), $Na_{0.5}Bi_{0.5}TiO_3$ (NBT), and $BaTiO_3$-$BiMeO_3$ (BT-BMe) based systems.

Barium titanate (BT) is one of the typical perovskite materials exhibiting an optimum dielectric permittivity along with outstanding ferroelectric properties. At the same time, it possesses a low Curie temperature and substantial remnant polarization which are not beneficial from an energy storage point of view. Efforts have been made in the past by some researchers to augment the properties of BT by using other ions as dopants. Substitution of Ca^{2+} at the A-site of the perovskite ($Ba_{0.7}Ca_{0.3}TiO_3$) gives a comparatively higher recoverable energy density of 1.41 J/cm^3 which is 40%

greater than pristine BT and moderate energy efficiency of 61% [17]. Similarly, the substitution of Zr^{4+} (existing only in one valance state) at the B-site which is already occupied by multivalent Ti ions (Ti^{3+} and Ti^{4+}) reduces the loss factor to a great extent by minimizing the electron hopping conduction between Ti^{3+} and Ti^{4+} [18]. Materials considered to be ideal for energy storage are often expected to be associated with high dielectric breakdown strength. Reducing the porosity and grain size with uniform grain size distribution may prove to be advantageous in such cases. In one of the research works, $Ba_{0.4}Sr_{0.6}TiO_3$ (a derivative of BT) was sintered in O_2 atmosphere to reduce the grain size down to 0.44 μm. sintering in O_2 forbids the creation of oxygen vacancies inhibiting grain growth. Breakdown strength of 16.72 kV/mm, the energy storage density of 1.0081 J/cm^3, and efficiency of 73.78% were achieved under this condition [19]. Sodium bismuth titanate or $Na_{0.5}Bi_{0.5}TiO_3$ (NBT) is another potential ferroelectric but a high remnant polarization (~39 μC/cm^2) and large leakage current hinder its energy storage performance. Several investigations have been focused on the development of NBT-based solid solutions and composites to improve their storage capability. Yao et al. [20] improved the storage properties of $0.9(0.94NBT\text{-}0.06BT)\text{-}0.1NaNbO_3$ by introducing ZnO as a dopant. Zn^{2+} ions in the B-site greatly boosted the dielectric constant (3218 at room temperature and 1 kHz) and increased the difference between remnant polarization and maximum polarization due to the local distortions of the perovskite unit cell.

3.2 Relaxor Ferroelectrics

Grain size, crystallite size, domain width, and defect structures are some crucial parameters to decide the storage properties of the materials. Conventional ferroelectrics even after modifications could attain a maximum energy storage efficiency of 50–60% owing to micrometer grain sizes and sub-micrometer domain widths. Domain wall mobility or switching which has a major contribution in determining the polarization behavior provides much less output in the case of optimized ferroelectric materials. An appropriate extension to the nanoworld is dispensed by relaxor ferroelectrics with nanoscale polarization disorders giving rise to natural nanometer-size polar structures even in bulk materials. These polar structures of polar nano regions (PNRs) are highly mobile and can dynamically change over several orders in response to external stimuli, e.g., electric field [21]. Being very small in feature size, these PNRs can flip easily on changing the direction of the applied electric field giving rise to slim $P-E$ loops, large maximum polarization, small remnant polarization, and moderate dielectric breakdown strength. Moreover, RFEs often exhibit fairly good temperature stability of energy storage properties due to their unique characteristic of diffuse phase transitions with temperature [22]. Few cases will be elaborated on here. Zhao et al. [23] modified BT (a known ferroelectric) by introducing $Bi(Ni_{2/3}Ta_{1/3})O_3$ as the end component which disrupted the long-range ferroelectric order of the parent compound into nano-sized PNRs. They noticed a crossover from FE to RFE with the

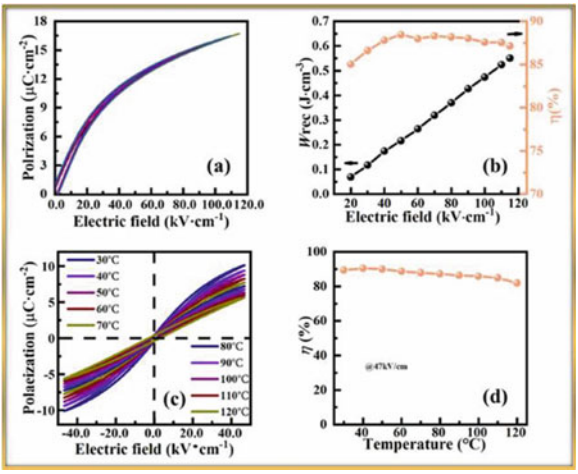

Fig. 4 **a** *P–E* loops **b** Recoverable energy density (W_{rec}) and η of $0.95BaTiO_3$-$0.05Bi_{0.5}Na_{0.5}TiO_3$ under different test electric fields; **c** *P–E* loops **d** η of $0.95BaTiO_3$-$0.05Bi_{0.5}Na_{0.5}TiO_3$ at 47 kV/cm in the temperature range 30 – 120 °C [23]

appearance of slim polarization hysteresis loops and extremely low remnant polarization. The composition with $0.05Bi(Ni_{2/3}Ta_{1/3})O_3$ demonstrated a recoverable energy density of 0.55 J/cm^3 with an efficiency of 87.15% at 117 kV/cm. In addition to that, the same composition also showed excellent temperature stability of energy storage properties (Fig. 4). Superior energy storage performance was observed in relaxor NBT-xBaZrO$_3$ compositional series with a slim polarization hysteresis loop and small remnant polarization. Besides, the replacement of Na^+ with higher valent Ba^{2+} reduces the grain size of the system gradually resulting in improved breakdown strength. With added advantages of excellent temperature stability and fatigue resistance, 0.75NBT-0.25BaZrO$_3$ displays a recoverable energy density of 1.56 J/cm^3 and high efficiency of 80.56% [24]. Similar studies have been conducted on NBT based systems to revamp the storage properties. In a ternary system based on NBT ((1-x)0.65NBT-0.35$Bi_{0.2}Sr_{0.7}TiO_3$)-xBaSnO$_3$), the addition of BaSnO$_3$ as an end member not only boosted the energy storage performance but also exhibited a thermally stable high dielectric constant. For 0.2 BaSnO$_3$, recoverable energy as high as 3.75 J/cm^3, efficiency 84.8%, and an outstanding power density of 38.73 MW/cm^3 could be achieved making it promising for pulsed power capacitor applications [25].

3.3 Antiferroelectrics

Antiferroelectrics is named so due to the presence anti parallel dipole moments and a zero net polarization, unlike ferroelectrics. Under substantially high electric field (AFE-FE phase switching field E_F), these antiparallel dipoles reorient themselves to form a ferroelectric phase producing macroscopic polarization. In most cases, it is a reversible transition since the FE phase again switches back to the AFE phase on reducing the applied field below E_A (field corresponding to FE-AFE transition).

Hence this unique category of materials posses double hystereses loop with almost a remnant polarization very close to zero and is very crucial in obtaining high recoverable energy and efficiency. Pb-based antiferroelectrics have been very attractive in this regard as they offer appreciable energy storage properties for practical applications [26]. However, research is in progress in full swing to find a suitable lead-free material at par with the pb-based materials. One of the lead-free antiferroelectric materials which owe much potential is $AgNO_3$. In 2016, undoped and Mn-doped $AgNO_3$ were reported to possess a high energy density > 2 J/cm^3 [27, 28]. Thereafter, Gao et al. [29] enhanced the AFE phase stability of this compound by La-doping. As expected, they could discover a very high energy density of 4.4 J/cm^3 and a moderate efficiency of 70% along with improved breakdown strength in 2 mol% La-doped $AgNO_3$. Similar modifications were also made by Zhao et al. and Han et al. [30, 31] (Fig. 5). Apart from that, NBT based systems when modified with some niobates also

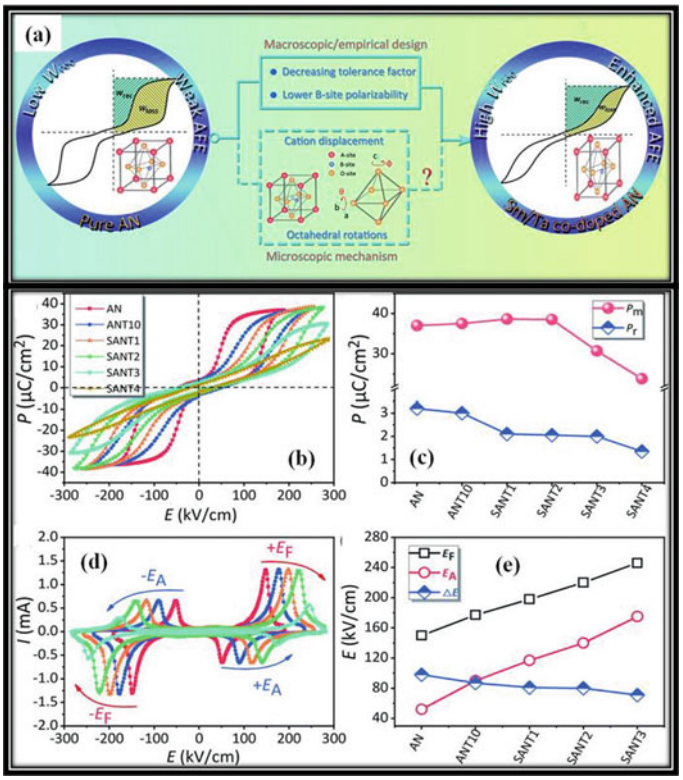

Fig. 5 **a** Representative diagram showing a strategy to improve recoverable energy in antiferroelectrics **b** polarization hysteresis loops **c** maximum and remnant polarization (P_m and P_r) **d** current (I) vs electric field **e** E_F, E_A and ΔE of AN, ANT10, SANT1, SANT2, SANT3 and SANT4 respectively.(Abbbriviations: $AgNbO_3$ (AN), $AgNb_{0.9}Ta_{0.1}O_3$ (ANT10) and $(Sm_xAg_{1-3x})(Nb_{0.9}Ta_{0.1})O_3$ (SANT1, SANT2, SANT3 for $x = 1, 2, 3, 4$ mol% respectively)) [31]

demonstrate fair energy storage properties. NBT-BT-KNN and NBT-$Ba_{0.5}K_{0.5}TiO_3$-KNN systems [32, 33] exhibit antiferroelectric-like behavior and adequate storage properties. But the energy storage performance is less appealing than $AgNO_3$ based systems. Nevertheless, adding $NaNbO_3$ (NN) as an end member to NBT showcased giant recoverable energy (W) of 7.02 J/cm^3 and efficiency (η) of 85%. In addition, NBT-0.22NN could maintain an optimum W > 3.5 J/cm^3 and η > 88% in the range 25–250 °C and 0.1–100 Hz making it a potential candidate for future pulsed power applications [34]. This may be attributed to the crossover of RFE of NBT to AFE relaxor phase with an increase in NN concentration making the AFE polarization loops slimmer and increasing the energy storage performance.

3.4 Glass–Ceramics

Though the energy storage density could be strengthened in FEs, RFEs, and AFEs by suitable modifications improving the dielectric breakdown strength (BDS) remains an issue, the lead-free materials (ceramics in particular) have a high concentration of defects which limits the BDS of the above-discussed ceramics. Factors such as porosity, grain size, charge transport, interfacial polarization, and the presence of secondary phases greatly influence the dielectric breakdown strength of the materials. Finer grain size with very little porosity is advantageous for obtaining high BDS. Some of the studies point out that introducing an appropriate amount of glass to the ceramics can substantially improve the BDS and thus maximizing the difference between maximum polarization and remnant polarization. Adding such glasses generates liquid phase sintering leading to grain refinement and large BDS. It is observed that B_2O_3-SiO_2 based glasses possess optimum electric durability and wettability due to which it acts as an effective additive for improving the performance of the parent composition [35]. Incorporation of 20 vol % of BaO-SiO_2-B_2O_3 glass into $Ba_{0.4}Sr_{0.6}TiO_3$ increased the dielectric breakdown strength of pristine ceramic from 12.1 to 23.9 kV/mm [36].

Wang et al. [37] made a detailed investigation on the effect of BaO-SrO-TiO_2-Al_2O_3-SiO_2-BaF_2 glass on grain size and BDS on barium titanate. They also noticed that BDS was related to charging transport across the grain boundaries in the space charge depletion region and was inversely proportional to the average field strength E_{GB} in the grain boundary space charge layer and is given by

$$E_{GB} = E\left(\frac{d_B}{d_{GB}}\right) \tag{10}$$

Here, E represents the externally applied electric field to the specimen; d_B and d_{GB} refer to the grain size and width of grain boundary space charge layer respectively. In yet another report, 0.5NBT-0.5ST ceramic was modified with glass addition (B_2O_3-Bi_2O_3-ZnO-SiO_2). With a glass content of 1wt, the energy density reached 1.67 J/cm^3 under a field strength of 200 kV/cm. The grain size was refined from 3.07 μmm to

0.98 μm without changing the phase structure and almost doubling the dielectric breakdown strength [38].

From the above discussions, it is now very clear that the dielectric and energy storage properties are largely dependent on the grain size of the ceramics/materials. The multilayer energy storage ceramic capacitors (MLESCC) which are widely preferred in the present time comprise hundreds of thin dielectric layers arranged in parallel with alternating interlayer metal electrodes. Usually, these dielectric layers are constructed from ceramics with high dielectric permittivity such a BT. Commercially available MLESCCs employ ~1 μm thick dielectric layers which require grain size of the order of 50–150 nm to meet the temperature stability and ensure reliable performance [39]. So, nanoscience or nanotechnology plays a vital role in this regard due to their unique properties as compared to the bulk. In the early stages single component nanomaterials were studied extensively but with rapid progress in technology, multi-component nanomaterials such as nanocomposites, thin films, core–shell structure, etc. due to diverse structure and composition. We will discuss a few of them here.

3.5 Core–Shell Structure

Core–shell structured materials have attracted the attention of the research community due to their extraordinary physical and chemical properties. Such structures are fabricated to overcome the hazards of densification in the case of nanomaterials. Considering the example of $BaTiO_3$, its nanocrystalline form (~30 nm) exhibits a slim and nearly linear *P–E* loop along with postponed saturation polarization and high dielectric breakdown strength dedicated to its fine grain size. On the other hand, it is very difficult to obtain high-density BT with a grain size maintained at the nanoscale (<100 nm) owing to easier grain growth in nanoparticles. Various synthesis techniques have been explored in the past to address this issue, e.g., spark plasma sintering, hot isostatic pressing, two-step sintering, etc. These listed methods accrue huge equipment costs, or the starting materials are monodisperse particles with sizes not greater than 10 nm. One of the alternatives adopted by Su et al. [40] was the introduction of a low melting glass as a coating on $BaTiO_3$ nanoparticles. The glass $65Bi_2O_3$-$20B_2O_3$-$15SiO_2$ forms a thin layer on commercially available BT nanoparticles forming a core–shell structure. The glass coating layer thickness could be adjusted by precursor concentrations and at an optimum loading of 26 vol% of borosilicate glass, no noticeable grain growth was obtained. This corroborates the fact that the coating acts as an effective grain growth inhibitor during the sintering process. The overall core–shell structure exhibited postponed saturation polarization and high dielectric breakdown strength of $\geq$ 1000 kV/cm. It also demonstrated a very high energy density of ~10 J/cm^3 which is much greater than bulk ceramics (Fig. 6).

In another study, $BaTiO_3$ nanoparticles were encapsulated in the FeO layer by the sol precipitation method. The FeO coating and secondary phase are crucial in impeding grain growth during sintering by infusing an effective diffusion

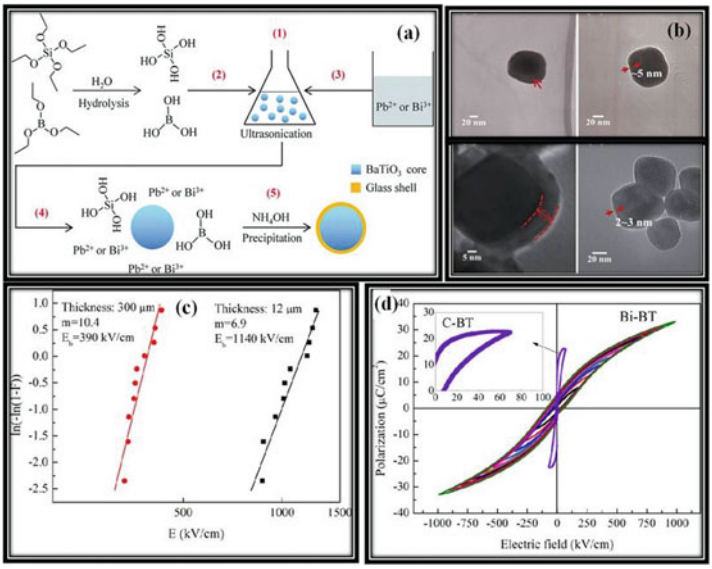

Fig. 6 **a** Representative diagram showing the formation of $BaTiO_3$/65Bi_2O_3-20B_2O_3-15SiO_2 glass core–shell structure **b** TEM micrographs indicating the thickness of the coating layer on the as-prepared nanoparticles **c** dielectric breakdown strength of the composite structure at two different thicknesses of 300 μm and 12 μm respectively **d** comparison of P – E loops for coarse-grained $BaTiO_3$ (C-BT) and glass coated composite (Bi-BT) [40]

layer. $BaTiO_3$@3%FeO nanoceramics displayed a high discharge energy density of 1.5 J/cm^3 at 300 kV/cm (8 times more than pristine BT), fast discharge features ($\tau_{0.9}$<1.5 μsec), excellent temperature (25–120 °C), and cyclic (up to 1 × 10^5 times) stability [41]. Similar work was performed by Huang et al. [42] in which they used SiO_2 to coat $Ba_{0.4}Sr_{0.6}TiO_3$ by wet-chemical process and then dense ceramics were fabricated out of the core–shell nanoparticles by spark plasma sintering. It was remarkable to note that the polarization decreased monotonously on increasing the amount of SiO_2 coating while the dielectric breakdown strength increased. $Ba_{0.4}Sr_{0.6}TiO_3$ ceramics with 8 mol% of SiO_2 exhibited a maximum energy storage density of 1.6 J/cm^3 at 400 kV/cm with an extremely high efficiency of 90.9%.

3.6 *Thick/Thin Films*

Another effective way of exploring the potential of nanotechnology is to incorporate the prospective nanoparticles as fillers in polymers to form thick/thin films. Such films have lesser defects as compared to their bulk counterparts and hence possess a high breakdown strength and energy storage density. For example, an

extraordinarily high recoverable energy density of 27 J/cm^3 in addition to breakdown strength of 1894 kV/cm was attained in Mn-doped 0.7NBT-0.3ST relaxor thin films grown on Pt/Ti/SiO_2/Si substrates synthesized through the sol–gel method [43]. $Sr_{0.6}(Na_{0.5}Bi_{0.5})_{0.4}Ti_{0.99}Mn_{0.01}O_3$ RFE thin films grown on the same substrate yield recoverable energy of 33.58 J/cm^3 along with appealing breakdown strength of 3134.3 kV/cm owing to less no. of oxygen vacancies [44]. Cheng et al. [45] observed ultra-high recyclable energy density in $Ba(Zr_{0.2}Ti_{0.8})O_3$ (BZT) ferroelectric films up to 166 J/cm^3 and efficiency up to 83% on reducing the film thickness to few nanometers. This is quite different from the typical FEs in the sense that the films show much-delayed saturation polarization which increases continuously from almost zero at remnant in a multipolar state to a substantial value under maximum applied field. Such a particular behavior may be attributed to the creation of an adaptive nanodomain structure in the perovskite films via phase engineering and strain tuning (Fig. 7). The reported film in this study is suitable for dielectric capacitors in energy storage, conditioning, and conversion. Films fabricated using physical methods ensure better crystalline quality and higher breakdown strength. One of the best examples is the attainment of a recoverable energy density of 154 J/cm^3 (applied field of 3500 kV/cm) in $(Bi_{1/2}Na_{1/2})_{0.9118}La_{0.02}Ba_{0.0582}(Ti_{0.97}Zr_{0.03})O_3$ epitaxial thin films deposited by pulsed laser deposition technique [46]. High epitaxial quality, optimum dielectric breakdown strength, and excellent relaxor dispersion are responsible for ultrahigh-energy storage in these thin films.

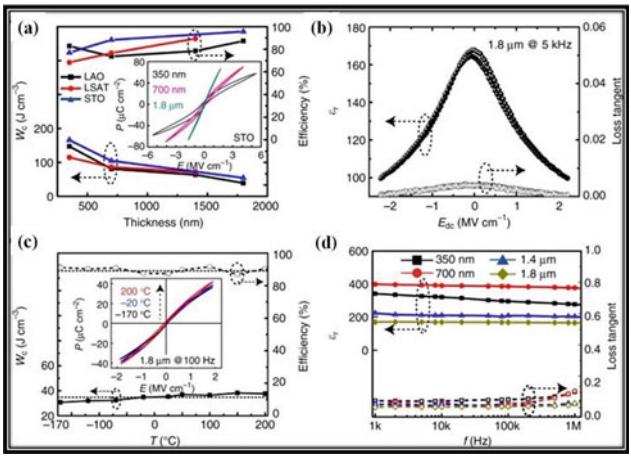

Fig. 7 **a** Variation of energy density (W_c), η and P – E loops with a thickness of BZT films grown on different substrates **b** room temperature variation of dielectric constant (ε_r) and loss tangent **c** (W_c), η and temperature-dependent P – E loops of 1.8 μm BZT film on LAO substrate **d** variation of ε_r and loss at the different thicknesses of BZT films grown on LAO [45]. (Abbreviations: $LaAlO_3$ (LAO), (La,Sr)(Al,Ta)O_3 (LSAT) and $SrTiO_3$ (STO))

3.7 Polymer Nanocomposites

Polymers are another category of materials that can give a tough competition to bulk and films in energy storage with an added advantage of wearability. Biaxial polypropylene (BOPP), polyphenylene sulfide (PPS), and polycarbonate (PC) are polymers that are already explored for commercial production. Despite that bottleneck for energy storage density is encountered and the problem of low permittivity, the inferior temperature stability of macromolecules has choked the pathway to practical applications. Hence, polymer nanocomposites with ceramics in the form of nanoparticles, nanofibers, and nanorods as fillers are more attractive as next-generation energy storage materials. Few instances describing the potential of polymer-ceramic nanocomposites as energy storage materials are cited here. It is a common observation that when ceramics nanofillers are incorporated into polymer matrix for building 0–3 or 1–3 structures; an improvement in permittivity and fairly better thermal stability may be expected. Boron nitride nanosheets (BNNSs) in P(VDF-TrFE-CFE) provide an insulating barrier to reduce the leakage current and lead to an enhancement in breakdown strength. The highest energy density and efficiency derived from this system were 20.3 J/cm^3 and 78% respectively. Further, its ternary counterparts with BT and BST were designed to achieve up gradation in dielectric breakdown strength by blocking electrical trees' development. Energy storage density of 21.1 J/cm^3 and η of 78% was achieved in P(VDF-CTFE)/12 wt% BNNS/15 wt% BT while for P(VDF-CTFE)/12 wt% BNNS/5 wt% BST, the featured values were 24.4 J/cm^3 and 76% respectively [47–49]. Hao et al. [50] in their work mentioned ultimate sized ferroelectric nanofillers, i.e., BT nanocrystals (prepared by TEG-sol method) in PVDF-co-hexafluro propylene (PVDF-HFP) matrix to enhance the breakdown strength and storage performance. They noticed highly enhanced breakdown strength (380 kV/mm) and maximal discharge energy density of 9.7 J/cm^3 at 30 vol% loadings of BT nanoparticles which were significantly higher than composites with coarse BT fillers (Fig. 8).

Nevertheless, the polymer-ceramic nanocomposites often suffer from poor interfacial compatibility and agglomeration of fillers which may affect the energy storage capacity. Surface modification and functionalization of the fillers are the most feasible solution to mitigate these issues. In a report by Gao et al. [51], BT nanoparticles were hydroxylated by H_2O_2 followed by a surface modification with DN-101 (a titanate coupling agent). They could notice an improvement in maximum polarization, breakdown strength, and discharge energy density in the treated nanocomposites as compared to the untreated ones. In another investigation, polydopamine (PDA) was employed to modify the surface of $BaSrTiO_3$ (BST) nanoparticles to increase the compatibility of ceramic fillers with polymer matrices. This technique remarkably elevated the dielectric breakdown strength of the nanocomposites to 466 MV/m, and at the same time, recoverable energy density was increased to 11 J/cm^3 which was almost 160% more than composites with unmodified BST [52]. Recently, sandwich nanocomposite structures have gained importance as they offer better performance features as compared to single-layer composites. Shen et al. [53]

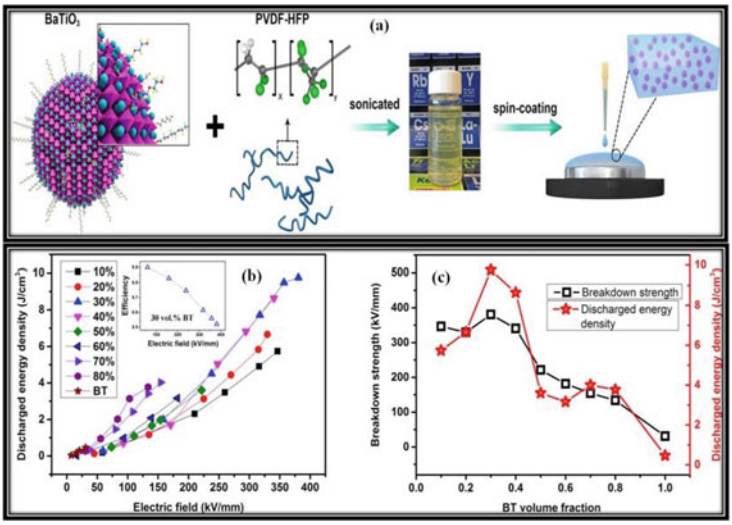

Fig. 8 **a** Representative diagram for the formation of BT/PVDF-HFP nanocomposite film **b** discharged energy density vs electric field at different vol% of BT **c** variation of breakdown strength and discharged energy density with vol% of BT [50]

implemented a comprehensive phase model to evaluate the breakdown strength of sandwich composite structures under electrostatic stimuli in this regard. Basing on the high-throughput results, they modeled a PVDF/BT nanocomposite sandwich with upper and lower layers filled with parallel nanosheets and middle layer filled with vertical nanofibers and obtained an energy density 2.44 times higher than virgin PVDF polymer (Fig. 9).

4 Summary

With the growing demands of modern society and the urgent need for securing our environment, lead-free energy storage devices have become indispensible. Nevertheless, research is rapidly progressing in this direction and it is expected that within few years lead-free materials to uproot the Pb-based in-framing energy storage devices. One of the most important figures of merit identified to strengthen the storage performance is these materials is recoverable/discharge energy density. As per the fundamental principles involved, enhancing the dielectric breakdown strength is the most effective way to improve the energy density. In addition to it, some of the applications require that the employed material should maintain its storage capacity in harsh conditions such as high temperature, and hence thermal stability is of utmost importance. So, in this chapter, we list the energy storage performance of different categories of prospective materials, oxides in particular, and their evolution from bulk to nanoscale.

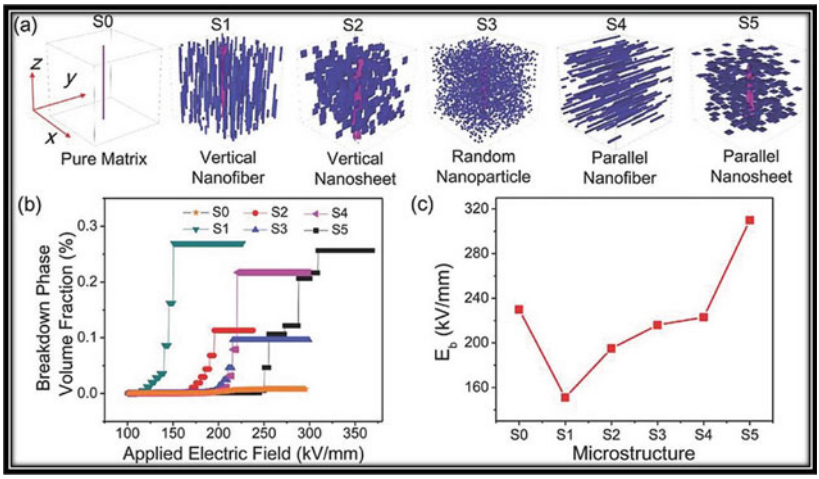

Fig. 9 **a** 3-D simulations of breakdown phase morphology in nanocomposites with different microstructures **b** evolution of breakdown phase volume fraction (10% except pure matrix) at applied electric fields **c** extracted breakdown strengths for corresponding nanocomposites [53]

Further, different methodologies which have proven to be achieving success in this context are also discussed. The first among them is domain engineering by inducing defects in both bulk and thin films suitable for polarization augmentation, particularly in the case of RFEs and AFEs. Another attempt that is of much importance is interfacial engineering employed in layered composites or core–shell structures and is essential to build stronger interfacial bonds for superior storage capabilities. The next one is downsizing the coarse grains into fine-grained structures which put a positive on the dielectric breakdown strength and indirectly on energy storage density. Moving ahead, we elaborated how the materials in their nano form exhibit exotic properties as compared to bulk due to minimal defects and surface properties. Ultra high energy densities, thermal stability, and breakdown strength could be achieved with core–shell structures and thin films. Sandwich polymer nanocomposites with optimum features are worthwhile for use in flexible electronics. Besides, phase-field simulation and first-principle calculations also provide evidence for experimental data and can give a projection for new generation energy storage materials. Thus, constant research efforts of the feature refining by implementation different synthesis techniques and utilization of computer simulation going hand in hand will sure give birth to more prospective and progressive materials to cater our future energy needs.

References

1. Key world energy statistics (2018) International Energy Agency
2. Rapier R (2020) Fossil Fuels Still Supply 84 Percent Of World Energy, June 2020— And

Other Eye Openers From BP's Annual Review. https://www.forbes.com/sites/rrapier/2020/06/20/bp-review-new-highs-in-global-energy-consumption-and-carbon-emissions-in-2019/?sh=4e2e94cf66a1
3. Yang L, Kong X, Li F, Hao H, Cheng Z, Liu H, Li JF, Zhang S (2019) Perovskite lead-free dielectrics for energy storage applications. Prog Mater Sci 102:72–108
4. Kusko A, DeDad J (2007) Stored energy-Short-term and long-term energy storage methods. IEEE Ind Appl Mag 13:66–72
5. Yao K, Chen S, Rahimabady M, Mirshekarloo MS, Yu S, Tay FEH, Sritharan T, Lu L (2011) Nonlinear dielectric thin films for high-power electric storage with energy density comparable with electrochemical supercapacitors. IEEE Trans Ultrason Ferroelectr Freq control 58:1968–1974
6. Jaffe B (1961) Antiferroelectric ceramics with field-enforced transitions: a new nonlinear circuit element. Proc IRE 49:1264–1267
7. Sun Z, Wang Z, Tian Y, Wang G, Wang W, Yang M, Wang X, Zhang F, Pu Y (2020) Progress, outlook, and challenges in lead-free energy-storage ferroelectrics. Adv Electron Mater 6:190069
8. Jin L, Li F, Zhang S (2014) Decoding the fingerprint of ferroelectric loops: Comprehension of the material properties and structures. J Am Ceram Soc 97:1–27
9. Chu BJ, Zhou X, Neese B, Zhang QM, Bauer F (2006) Relaxor ferroelectric poly(vinylidene fluoride-trifluoroethylene-chlorofluoroethylene) terpolymer for high energy density storage capacitors. IEEE Trans Dielectr Electr Insul 13:1162–1169
10. Hao X (2013) A review on the dielectric materials for high energy-storage application. J Adv Dielectr 3:1330001
11. Love GR (1990) Energy storage in ceramic dielectrics. J Am Ceram Soc 73:323–328
12. Li F, Yang K, Liu X, Zou J, Zhai J, Shen B, Li P, Shen J, Liu B, Chen P, Zhao K (2017) Temperature induced high charge–discharge performances in lead-free $Bi_{0.5}Na_{0.5}TiO_3$-based ergodic relaxor ferroelectric ceramics. Scr Mater 141:15–19
13. Tang H, Lin Y, Sodano HA (2013) Synthesis of high aspect ratio $BaTiO_3$ nanowires for high energy density nanocomposite capacitors. Adv Energy Mater 3:451–456
14. Chen X, Zhang H, Cao F, Wang G, Dong X, Gu Y, He H, Liu Y (2009) Charge-discharge properties of lead zirconate stannate titanate ceramics. J Appl Phys 106:034105
15. Xu C, Liu Z, Chen X, Yan S, Cao F, Dong X, Wang G (2016) High charge-discharge performance of $Pb_{0.98}La_{0.02}(Zr_{0.35}Sn_{0.55}Ti_{0.10})_{0.995}O_3$ antiferroelectric ceramics. J Appl Phys 120:074107
16. Ulrich R, Schaper L, Nelms D, Leftwich M (2000) Comparison of paraeletric and ferroelectric materials for applications as dielectrics in thin film integrated capacitors. Int J Microcircuits Electron Packag 23:172–181
17. Puli VS, Pradhan DK, Riggs BC, Chrisey DB, Katiyar RS (2014) Structure, ferroelectric, dielectric and energy storage studies of $Ba_{0.70}Ca_{0.30}TiO_3$, $Ba(Zr_{0.20}Ti_{0.80})O_3$ ceramic capacitors. Integr Ferroelectr 157:139–146
18. Eoh YJ, Kim E (2015) Dependence of dielectric properties on microstructural characteristics of $(Ba_{0.7}Sr_{0.25}Ca_{0.05})(Ti_{0.9}Zr_{0.1})O_3$ ceramics. Ceram Int 41:S2–S8
19. Jin Q, Pu YP, Wang C, Gao ZY, Zheng HY (2017) Enhanced energy storage performance of $Ba_{0.4}Sr_{0.6}TiO_3$ ceramics: influence of sintering atmosphere. Ceram Int 43:S232–S238
20. Yao Y, Li Y, Sun N, Du J, Li X, Zhang L, Zhang Q, Hao X (2018) Enhanced dielectric and energy-storage properties in ZnO-doped $0.9(0.94Na_{0.5}Bi_{0.5}TiO_3-0.06BaTiO_3)-0.1NaNbO_3$ ceramics. Ceram Int 44:5961–5966
21. Shvartsman VV, Lupascu DC (2012) Lead-free relaxor ferroelectrics. J Am Ceram Soc 95:1–26
22. Zheng DG, Zuo RZ, Zhang DS, Li Y (2015) Novel $BiFeO_3$-$BaTiO_3$-$Ba(Mg_{1/3}Nb_{2/3})O_3$ lead-free relaxor ferroelectric ceramics for energy-storage capacitors. J Am Ceram Soc 98:2692–2695
23. Zhao H, Yang X, Pang D, Long X (2021) Enhanced energy storage efficiency by modulating field-induced strain in $BaTiO_3$-Bi $(Ni_{2/3}Ta_{1/3})$ O_3 lead-free ceramics. Ceram Int
24. Yu Y, Zhang Y, Zhang Y, Li H, Zhang Q, Lu Y, He Y (2020) High-temperature energy storage performances in $(1-x)(Na_{0.50}Bi_{0.50}TiO_3)$-$xBaZrO_3$ lead-free relaxor ceramics. Ceram Int 46:28652–28658

25. Shi P, Zhu X, Lou X, Yang B, Guo X, He L, Liu Q, Yang S, Zhang X (2021) $Bi_{0.5}Na_{0.5}TiO_3$-based lead-free ceramics with superior energy storage properties at high temperatures. Compos B Eng 215:108815
26. Zhang Y, Liu P, Shen M, Li W, Ma W, Qin Y, Zhang H, Zhang G, Wang Q, Jiang S (2020) High energy storage density of tetragonal PBLZST antiferroelectric ceramics with enhanced dielectric breakdown strength. Ceram Int 46:3921–3926
27. Tian Y, Jin L, Zhang H, Xu Z, Wei X, Politova ED, Stefanovich SY, Tarakina NV, Abrahams I, Yan H (2016) High energy density in silver niobate ceramics. J Mater Chem A 4:17279–17287
28. Zhao L, Liu Q, Zhang S, Li JF (2016) Lead-free $AgNbO_3$ anti-ferroelectric ceramics with an enhanced energy storage performance using MnO_2 modification. J Mater Chem C 4:8380–8384
29. Gao J, Zhang Y, Zhao L, Lee KY, Liu Q, Studer A, Hinterstein M, Zhang S, Li JF (2019) Enhanced antiferroelectric phase stability in La-doped $AgNbO_3$: perspectives from the microstructure to energy storage properties. J Mater Chem A 7:2225–2232
30. Zhao L, Gao J, Liu Q, Zhang S, Li JF (2018) Silver niobate lead-free antiferroelectric ceramics: enhancing energy storage density by B-site doping. ACS Appl Mater Interfaces 10:819–826
31. Han K, Luo N, Mao S, Zhuo F, Liu L, Peng B, Chen X, Hu C, Zhou H, Wei Y (2019) Ultrahigh energy-storage density in A-/B-site co-doped $AgNbO_2$ lead-free antiferroelectric ceramics: insight into the origin of antiferroelectricity. J Mater Chem A 7:26293–26301
32. Ding J, Liu Y, Lu Y, Qian H, Gao H, Chen H, Ma C (2014) Enhanced energy-storage properties of 0.89 $Bi_{0.5}Na_{0.5}TiO_3$–0.06$BaTiO_3$–0.05$K_{0.5}Na_{0.5}NbO_3$ lead-free anti-ferroelectric ceramics by two-step sintering method. Mater Lett 114:107–110
33. Hao J, Xu Z, Chu R., Li W, Juan D, Peng F (2015) Enhanced energy-storage properties of $(1-x)[(1-y)(Bi_{0.5}Na_{0.5})TiO_3$–$y(Bi_{0.5}K_{0.5})TiO_3]$–$x(K_{0.5}Na_{0.5})NbO_3$ lead-free ceramics. Solid State Commun 204:19–22
34. Qi H, Zuo R (2019) Linear-like lead-free relaxor antiferroelectric $(Bi_{0.5}Na_{0.5})TiO_3$–$NaNbO_3$ with giant energy-storage density/effiffifficiency and super stability against temperature and frequency. J Mater Chem A 7:3971–3978
35. Divya PV, Kumar V (2007) Crystallization studies and properties of $(Ba_{1-x}Sr_x)TiO_3$ in borosilicate glass. J Am Ceram Soc 90:472–476
36. Zhang QM, Wang L, Luo J, Tang Q, Du J (2009) Improved energy storage density in barium strontium titanate by addition of BaO-SiO_2-B_2O_3 glass. J Am Ceram Soc 92:1871–1873
37. Wang XR, Zhang Y, Song XZ, Yuan ZB, Ma T, Zhang Q, Deng CS, Liang TX (2012) Glass additive in barium titanate ceramics and its influence on electrical breakdown strength in relation with energy storage properties. J Eur Ceram Soc 32:559–567
38. Liu G, Wang Y, Han G, Gao J, Yu L, Tang M, Li Y, Hu J, Jin L, Yan Y (2020) Enhanced electrical properties and energy storage performances of NBT-ST Pb-free ceramics through glass modification. J Alloys Compd 836:154961
39. Cai Z, Wang X, Hong W, Luo B, Zhao Q, Li L (2018) Grain-size–dependent dielectric properties in nanograin ferroelectrics. J Am Ceram Soc 101:5487–5496
40. Su X, Riggs BC, Tomozawa M, Nelson JK, Chrisey DB (2014) Preparation of $BaTiO_3$/low melting glass core–shell nanoparticles for energy storage capacitor applications. J Mater Chem A 2:18087–18096
41. Wang H, Cao M, Tao C, Hao H, Yao Z, Liu H (2021) Tuning the microstructure of $BaTiO_3$@FeO core-shell nanoparticles with low temperatures sintering dense nanocrystalline ceramics for high energy storage capability and stability. J Alloys Compd 864:158644
42. Huang YH, Wu YJ, Liu B, Yang TN, Wang JJ, Li J, Chen LQ, Chen XM (2018) From core–shell $Ba_{0.4}Sr_{0.6}TiO_3$@SiO_2 particles to dense ceramics with high energy storage performance by spark plasma sintering. J Mater Chem A 6:4477–4484
43. Zhang YL, Li WL, Cao WP, Feng Y, Qiao YL, Zhang TD, Fei WD (2017) Mn doping to enhance energy storage performance of lead-free 0.7NBT-0.3ST thin films with weak oxygen vacancies. Appl Phys Lett 110:243901
44. Zhang YL, Li WL, Qiao YL, Zhao Y, Wang ZY, Yu Y, Xia HT, Li Z, Fei WD (2018) 0.6ST-0.4NBT thin film with low level Mn doping as a lead-free ferroelectric capacitor with high energy storage performance. Appl Phys Lett 112:093902

45. Cheng H, Ouyang J, Zhang YX, Ascienzo D, Li Y, Zhao YY, Ren Y (2017) Demonstration of ultra-high recyclable energy densities in domain-engineered ferroelectric films. Nat Commun 8:1–7
46. Peng B, Zhang Q, Li X, Sun T, Fan H, Ke S, Ye M, Wang Y, Lu W, Niu H, Scott JF (2015) Giant electric energy density in epitaxial lead-free thin films with coexistence of ferroelectrics and antiferroelectrics. Adv Electr Mater 1:1500052
47. Li Q, Zhang G, Liu F, Han K, Gadinski MR, Xiong C, Wang Q (2015) Solution-processed ferroelectric terpolymer nanocomposites with high breakdown strength and energy density utilizing boron nitride nanosheets. Energy Environ Sci 8:922–931
48. Wang G, Li J, Zhang X, Fan Z, Yang F, Feteira A, Zhou D, Sinclair DC, Ma T, Tan X, Wang D (2019) Ultrahigh energy storage density lead-free multilayers by controlled electrical homogeneity. Energy Environ Sci 12:582–588
49. Liu F, Li Q, Li Z, Dong L, Xiong C, Wang Q (2018) Ternary PVDF-based terpolymer nanocomposites with enhanced energy density and high power density. Compos Part A: Appl Sci Manuf 109:597–603
50. Hao Y, Wang X, Bi K, Zhang J, Huang Y, Wu L, Zhao P, Xu K, Lei M, Li L (2017) Significantly enhanced energy storage performance promoted by ultimate sized ferroelectric $BaTiO_3$ fillers in nanocomposite films. Nano Energy 31:49–56
51. Gao L, He JL, Hu J, Li Y (2014) Large enhancement in polarization response and energy storage properties of poly(vinylidene fluoride) by improving the interface effect in nanocomposites. J Phys Chem C 118:831–838
52. Xie YC, Jiang WR, Fu T, Liu JJ, Zhang ZC, Wang SN (2018) Achieving high energy density and low loss in PVDF/BST nanodielectrics with enhanced structural homogeneity. ACS Appl Mater Interfaces 10:29038–29047
53. Shen ZH, Wang JJ, Lin YH, Nan CW, Chen LQ, Shen Y (2018) High-throughput phase-field design of high-energy-density polymer nanocomposites. Adv Mater 30:1704380